A Novel Indoor Positioning Technique Using Magnetic Fingerprint Difference

Binhee Kim, *Member, IEEE*, and Seung-Hyun Kong, *Senior Member, IEEE*

***Abstract*— Utilizing the pattern of magnetic field intensity (MFI) variation over a distance as a fingerprint for indoor positioning of mobile devices has gained increasingly wide attention. However, pattern matching with a large fingerprint is computationally expensive, and magnetometers are vulnerable to ferromagnetic perturbations and prone to have unknown magnetic offset (MO) in MFI measurements, which may result in large positioning error. In addition, the time-varying attitude of mobile devices and unreliable attitude determination with power consuming gyroscopes in mobile devices can render the 3-D MFI measurement useless for indoor positioning. In this paper, we propose a low power consuming and computationally efficient indoor positioning technique using the difference in 2-D (horizontal and vertical) MFI measurements that are collected over a distance, where 3-D accelerometers are used to find the vertical direction, and the MFI measurement difference is used to enhance robustness to unknown MO fixed in the body frame but time varying due to user dynamics in the navigation frame. The analysis of real data verifies that the proposed technique affords superior positioning performance relative to the conventional magnetic fingerprint techniques and achieves a similar performance to the conventional magnetic fingerprint techniques with MO-free measurements.**

***Index Terms*— Accelerometer, fingerprint, indoor positioning, magnetic positioning, smartphone.**

I. Introduction

RECENTLY, demands for location-based service (LBS) in indoor environments are increasing rapidly as expected given that the majority of mobile users are in indoor environments. To meet the demands for indoor LBS, a number of indoor positioning techniques have been introduced in the literature. These include, for example, indoor positioning techniques using time of arrival, time difference of arrival, angle of arrival, received signal strength, and the fingerprint of radio signals such as global positioning system, cellular communication systems, Wi-Fi, ultrawideband (UWB), and Zigbee [1]–[3]. Other indoor positioning techniques use camera vision [4], magnetometers [5], and inertial sensors [6].

Despite the large number of indoor positioning techniques, indoor LBS is not yet ubiquitously available; the radio-based techniques require a dense deployment of transmitters all over the indoor area of interest for high accuracy. Furthermore, nonradio-based techniques are not reliable or they are computationally expensive, for example, inertial navigation system [6], [7] requires frequent error correction due to diverging errors and the camera vision based navigation [4] is computationally expensive and the performance depends on the illumination condition.

Magnetic sensing for indoor positioning is an emerging technique and has been currently used for robot navigation on a flat floor [8]. On the basis of three-axis magnetometers being embedded in smartphones, a number of studies have sought to utilize magnetometer measurements for indoor positioning [5], [9], [10]. Researchers have found that the magnetic field intensity (MFI) in indoor environments varies from 20 to 80 μT and is sufficiently stable, i.e., the variation of the intensity at a location over time is negligible [9], [11], and the pattern of the MFI variation over a distance is unique and consequently locating a mobile device is possible by pattern matching of the MFI measurements, i.e., the magnetic fingerprint [9], [12] of the indoor environment.

However, using MFI measurements from smartphones for indoor positioning accompanies a few notable problems, while MFI at a particular indoor location is a 3-D stationary vector in space, the attitude of a smartphone varies depending on the user's motion, and utilizing the three-axis gyroscope to find the time-varying attitude of the smartphone consumes several times larger power consumption than a three-axis accelerometer and a three-axis magnetometer in a smartphone [13], [14]. In addition, the magnetometers in smartphones are vulnerable to external magnetic perturbations, which often result in a magnetic distortion known as soft and hard iron effects [15]. Soft iron distortion (SID) is caused by induced fields from any ferromagnetic material [16], [17]. However, SID may be small for smartphones when magnetometers are carefully designed to be negligibly impacted by other electromagnetic circuits in the phone [17]–[20]. Hard iron distortion (HID) occurs due to ferromagnetic materials such as the magnets of audio speakers and buzzers [16], [17], [21], which causes a 3-D magnetic offset (MO) in magnetometer measurements that may be not negligible. The SID and HID are analyzed in [15] and the MO is observed in field measurements [9]. In [18], the levels of SID and HID observed in practice are 1 μT and larger than 5 μT, respectively. To compensate for MO, a number of techniques have been introduced in the literature. The conventional eight-shape-loop motion-based MO calibration requires user's labor for 1 min or more [22] before we use the three-axis magnetometers. Other calibration techniques

Manuscript received September 3, 2015; revised February 27, 2016; accepted March 28, 2016. Date of publication June 8, 2016; date of current version August 9, 2016. This work (2013R1A2A2A01067863) was supported by Mid-career Researcher Program through NRF grant funded by the Korean government (MEST). The Associate Editor coordinating the review process was Dr. Dario Petri. *(Corresponding author: Seung-Hyun Kong.)*

The authors are with the CCS Graduate School for Green Transportation, Korea Advanced Institute of Science and Technology, Daejeon 305-701, South Korea (e-mail: vini@kaist.ac.kr; skong@kaist.ac.kr).

Color versions of one or more of the figures in this paper are available online at http://ieeexplore.ieee.org.

Digital Object Identifier 10.1109/TIM.2016.2566759

are computationally expensive [18] or require extra knowledge of the magnetic field at the location of interest [23]. The third problem is that there are indoor environments where MFI varies significantly, for example, subway stations, due to the trains. Finally, pattern matching algorithms for large fingerprint data collected over a distance are computationally expensive [24].

In this paper, we assume that the attitude variation of the smartphone is small, for example, when the mobile device is placed on a moving cart or when the user is moving while looking at the mobile device in hand. The change in the user velocity occurs only locally and sparsely during the collection of measurements over a distance, since a user may not change the walking velocity or the direction all the time. In addition, we consider indoor environments with no significantly varying MFI over time. While this may limit the application of the proposed technique, most in-building and in-house environments have stationary MFI [9]. Since the HID is larger than the SID in smartphones and is one of the dominant errors on the magnetic finger printing based positioning [18], [19], we assume the constant MO in this paper.

With the above assumptions, we propose a magnetic fingerprint-based indoor positioning technique that has important advantages over the conventional techniques, such as robustness to the small attitude variation of smartphones and unknown MO, low power consumption, and low computational cost. The proposed technique does not use the power-consuming and unreliable three-axis gyroscopes to find the attitude of the smartphone but uses low-power-consuming three-axis accelerometers to find the direction of gravity, which is used to estimate the vertical and horizontal (i.e., 2-D) MFI components from the three-axis magnetometer measurements. In fact, this scheme has already been introduced by Li *et al.* [9] and Yun *et al.* [25] conceptually, where they discuss that three-axis accelerometers in smartphones can be used to detect the direction of gravity and that it is possible to reliably extract the vertical and horizontal MFI measurements. To mitigate the effect of the unknown MO on fingerprint-based positioning, the proposed technique employs forward difference of the estimated vertical and horizontal MFI components that are collected over a short distance (e.g., less than 10 m). As analyzed and verified with real data, the proposed forward measurement difference (MD) provides strong robustness to the unknown MO and convenience to the user at negligible time and computational costs. The third advantage is that the proposed technique uses a low computational and fast pattern matching algorithm for the 2-D (i.e., vertical and horizontal) magnetic fingerprint difference. We demonstrate that the computational cost reduction with the proposed technique is significant.

The rest of this paper is organized as follows. In Section II, we show that the pattern matching technique with magnetic MD is much more robust to unknown fixed (time-invariant) or time-varying MOs than the conventional pattern matching techniques. The pattern matching algorithm using the MD is proposed in Section III, and we introduce a conventional Bayesian positioning filter [4] to test the proposed technique with field measurements. The positioning performance of the proposed technique is compared with those of the conventional techniques with unknown MO and with those with no MO in Section IV. Our conclusion is presented in Section V.

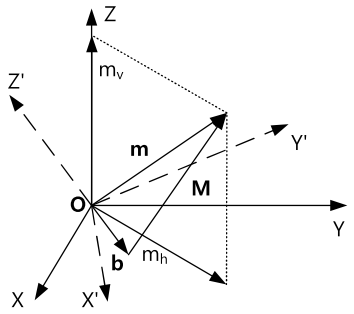

Fig. 1. Vertical and horizontal measurements with offset **b**.

Throughout this paper, we use bold letter(s) to represent vectors and matrices, and the following acronyms are used: MFI, MD, MO, map database (MDB), and signal-to-offset-distortion ratio (SOR). In this paper, $(\cdot)_v$ and $(\cdot)_h$ denote the vertical and horizontal components, respectively. And $(\cdot)^{(a_v)}$ denotes the conventional amplitude-based pattern matching technique (conventional Amp. technique) for time-varying MO, $(\cdot)^{(a_f)}$ denotes the conventional Amp. technique for time-invariant MO, $(\cdot)^{(m_v)}$ denotes the proposed MD-based pattern matching technique (proposed MD technique) for time-varying MO, and $(\cdot)^{(m_f)}$ denotes the proposed MD technique for time-invariant MO.

II. Forward Measurement Difference

In this section, we analyze the pattern matching performance with MD and compare the performance with that of the conventional pattern matching technique for time-invariant and time-varying MOs in terms of SOR. Since the proposed MD technique uses the vertical and horizontal MFI measurements for positioning, poor (or no) estimation of the dynamics of mobile device causes the direction of the MO bias vector **b** to change over time. Therefore, it is necessary to verify the robustness of the proposed MD technique to MO for cases when the attitude of the mobile device is varying and unknown to the positioning algorithm and where the attitude of the mobile device is fixed and known to the positioning algorithm.

Let $\mathbf{m} = \{m_x, m_y, m_z\}$ be an MFI vector measured by the three-axis magnetometers in the body frame of a smartphone, represented by the $x'y'z'$-coordinate, for an unknown offset **b** and the true MFI vector **M** as shown in Fig. 1, where the navigation frame is represented by the xyz-coordinate. Due to the user's motion and the quickly diverging errors in the cheap three-axis gyroscope in the smartphone, the roll, pitch, and yaw angles of the body frame with respect to the navigation frame become unreliable after a small time interval [7]. However, when a three-axis accelerometer can reliably find the direction of gravity **g** [9], [25], the vertical amplitude and the horizontal magnitude of the MFI are found as

$$m_v = \mathbf{m} \odot (-\mathbf{g}/|\mathbf{g}|) + w_v \tag{1}$$

$$m_h = \left|\mathbf{m} - m_v(-\mathbf{g}/|\mathbf{g}|)\right| + w_h \tag{2}$$

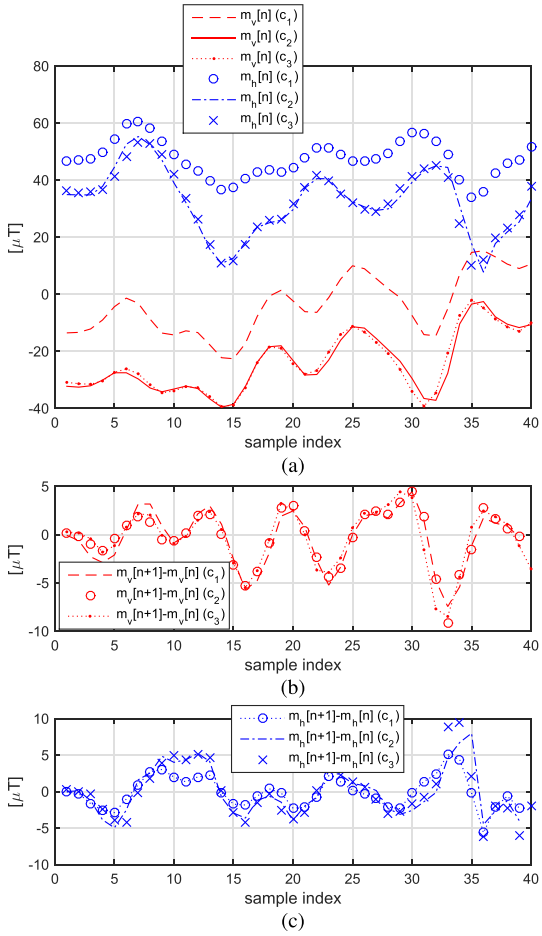

Fig. 2. Amplitude and MD patterns in real environments. (a) Measurement amplitudes. (b) Forward MDs for m_v. (c) Forward MDs for m_h.

where $\odot$ denotes the vector inner product operation and w_v and w_h represent the small measurement errors due to the noise and the direction estimation error of $\mathbf{g}$, respectively. We assume that w_v and w_h have a zero-mean Gaussian distribution with variances σ_v^2 and σ_h^2, respectively [23]. Since noise in the three orthogonal axes of the $x'y'z'$-coordinate have a similar power, we assume that $\sigma_h^2 = 2\sigma_v^2$ in this paper.

Let b_v and b_h represent the vertical and horizontal amplitudes of the unknown MO $\mathbf{b}$, respectively. Note that $\mathbf{b}$ is assumed as a constant in the body frame, while b_v and b_h are in the navigation frame. When the user is walking with the smartphone in his/her hand, the attitude of the magnetometer ($x'y'z'$-coordinate) is changing, and consequently, the direction of the MO $\mathbf{b}$ is time varying in the navigation frame. Therefore, for an example, two independent three-axis magnetometers embedded in two different smartphones undergoing different dynamics may produce completely different MFI measurements for the same MFI $\mathbf{M}$. In general, when a user is walking with a smartphone in his/her hand, m_v and m_h are changing due to the change in $\mathbf{M}$, and $\mathbf{b}$ is changing due to the user dynamics.

Fig. 2 shows m_v and m_h measurements (at 10 Hz) obtained with a smartphone (Samsung Galaxy S5) along the same straight path in a building, where c_1 represents the first measurement with the smartphone on a tablet PC, c_2 represents the second measurement with the smartphone alone 20 min later than c_1, and c_3 represents the third measurement with the smartphone alone 20 min later than c_2. Fig. 2(a) shows that c_2 and c_3 have very similar MFI patterns, and c_1 shows a similar envelope pattern but with large mean offset. However, Fig. 2(b) and (c) shows that the forward MDs for m_v and m_h measurements have very similar patterns in c_1, c_2, and c_3. As shown, there are significant MOs from 5 to 20 μT in both the vertical and horizontal measurements, and as a result, the amplitude-based matching between the two plots at different time can be obscured.

A. Varying Attitude of Mobile Device

In the following analysis, we show the superior robustness of the proposed MD technique, i.e., the proposed MD technique, to unknown MO through the comparison with the conventional Amp. technique in terms of the SOR, when the attitude of smartphone is unknown and time varying. However, we assume that due to the help of the accelerometer, estimating the direction of gravity is successful and reliable, and hence, measuring m_v and m_h (not M_v and M_h, the true vertical and horizontal MFI components) is successful. In the following, $s_{(\cdot)}$ denotes the MO-free MFI measurements stored in the MDB. Since the noise $\|\mathbf{w}\|$ is much smaller than the (MO) bias $\|\mathbf{b}\|$, we assume that the effect of noise on the pattern matching is small and negligible compared with that of the bias in this paper.

For the conventional Amp. technique, a correlation output between m_v and s_v is expressed as

$$\begin{aligned} z_v^{(a_v)}[n] &= (M_v[n] + b_v[n])s_v[n] \\ &= M_v[n]s_v[n] + b_v[n]s_v[n] \\ &= M_v^{(a_v)}[n] + B_v^{(a_v)}[n] \end{aligned} \tag{3}$$

where $M_v^{(a_v)}[n] = M_v[n]s_v[n]$, $B_v^{(a_v)}[n] = b_v[n]s_v[n]$, and n represents the time index of the measurement at $t = nT_s$. In the case of time-varying vertical MO due to the unknown dynamics of the mobile device, the offset–distortion component $B_v^{(a_v)}$ has a zero-mean Gaussian distribution [23] with variance

$$\mathrm{Var}\big(B_v^{(a_v)}[n]\big) = E\big[b_v^2[n]s_v^2[n]\big]. \tag{4}$$

The correlation output between the magnitudes m_h and s_h is

$$\begin{aligned} z_h^{(a_v)}[n] &= \big[(M_{hx}[n] + b_{hx}[n])^2 + (M_{hy}[n] + b_{hy}[n])^2\big] \\ &\quad \times (s_{hx}^2[n] + s_{hy}^2[n]) \\ &= M_h^{(a_v)}[n] + B_h^{(a_v)}[n] \end{aligned} \tag{5}$$

where

$$M_h^{(a_v)}[n] = \big(M_{hx}^2[n] + M_{hy}^2[n]\big)\big(s_{hx}^2[n] + s_{hy}^2[n]\big) \tag{6a}$$

$$\begin{aligned} B_h^{(a_v)}[n] = \big[&2(M_{hx}[n]b_{hx}[n] + M_{hy}[n]b_{hy}[n]) \\ &+ (b_{hx}^2[n] + b_{hy}^2[n])\big]\big(s_{hx}^2[n] + s_{hy}^2[n]\big) \end{aligned} \tag{6b}$$

and $(\cdot)_{hx}$ and $(\cdot)_{hy}$ denote the MFIs for the x-axis and the y-axis in the horizontal plane, respectively. From (6b), it is

found that the offset–distortion component $B_h^{(a_v)}$ has a nonzero mean and variance as

$$E\big[B_h^{(a_v)}[n]\big] = E\big[b_{hx}^2[n] + b_{hy}^2[n]\big]E\big[s_{hx}^2[n] + s_{hy}^2[n]\big] \quad (7a)$$

$$\begin{aligned}\mathrm{Var}\big(B_h^{(a_v)}[n]\big) = {} & E\big[(s_{hx}^2[n] + s_{hy}^2[n])^2\big] \\ & \times\big(2E\big[b_h^4[n]\big] + 2E\big[b_h^2[n]\big]E\big[b_h^2[n]\big] \\ & \quad + 8E\big[M_h^2[n]\big]E\big[b_h^2[n]\big]\big) \\ & - 2E\big[(s_{hx}^2[n] + s_{hy}^2[n])\big]E\big[b_h^2[n]\big] \end{aligned} \quad (7b)$$

respectively, where

$$E\big[b_h^4[n]\big] = E\big[b_{hx}^4[n]\big] = E\big[b_{hy}^4[n]\big] \quad (8a)$$

$$E\big[b_h^2[n]\big] = E\big[b_{hx}^2[n]\big] = E\big[b_{hy}^2[n]\big] \quad (8b)$$

$$E\big[M_h^2[n]\big] = E\big[M_{hx}^2[n]\big] = E\big[M_{hy}^2[n]\big]. \quad (8c)$$

As a result, in the presence of a time-varying MO, the variance of the vertical offset–distortion component (4) divided by the power of the vertical signal component $M_v^{(a)}[n]$ for the conventional Amp. technique is obtained as

$$P_v^{(a_v)}[n] = E\big[b_v^2[n]s_v^2[n]\big]/E\big[s_v^2[n]\big]. \quad (9)$$

In addition, the variance of horizontal offset–distortion component (4) divided by the power of the horizontal signal component $M_h^{(a)}[n]$ is derived as

$$\begin{aligned} P_h^{(a_v)}[n] = {} & \big(2E\big[b_h^4[n]\big] + 2E\big[b_h^2[n]\big]E\big[b_h^2[n]\big] \\ & + 8E\big[M_h^2[n]\big]E\big[b_h^2[n]\big]\big) \\ & - \left(\frac{2E\big[s_{hx}^2[n] + s_{hy}^2[n]\big]E\big[b_h^2[n]\big]}{E\big[(s_{hx}^2[n] + s_{hy}^2[n])^2\big]}\right) \end{aligned} \quad (10a)$$

$$\begin{aligned} \simeq {} & 2E\big[b_h^4[n]\big] + 2E\big[b_h^2[n]\big]E\big[b_h^2[n]\big] \\ & + 8E\big[M_h^2[n]\big]E\big[b_h^2[n]\big]. \end{aligned} \quad (10b)$$

Since the second $(\cdot)$ term in (10a) is negligibly small compared with the first $(\cdot)$ term in (10a), $P_h^{(a_v)}$ can be approximated by (10b).

For the proposed MD technique, in the presence of a time-varying MO, the variance of the vertical offset–distortion component is zero as found in (13), so that

$$P_v^{(m_v)}[n] = 0 \quad (11)$$

and the variance of the horizontal offset–distortion component (16b) divided by the horizontal signal component (15a) is found as

$$\begin{aligned} P_h^{(m_v)}[n] = {} & E\big[4b_{hx}^2[n](M_{hx}[n+1] - M_{hx}[n])^2\big] \\ & + E\big[4b_{hy}^2[n](M_{hy}[n+1] - M_{hy}[n])^2\big] \\ = {} & 4E\big[b_h^2[n]\big]\big[(M_{hx}[n+1] - M_{hx}[n])^2 \\ & + (M_{hy}[n+1] - M_{hy}[n])^2\big]. \end{aligned} \quad (12)$$

In general, since the dynamics of a mobile device in an indoor area is slow enough compared with the measurement rate R_M, the MOs in the two consecutive magnetometer measurements are almost the same. However, when the R_M is too high, the MD may be fail to show the variation in the MFI components, while when the R_M is too low, the time-varying MO may be not canceled out enough. Therefore, R_M should be properly set (10 Hz $\leq R_M \leq$ 20 Hz for magnetometers in smartphones). If the R_M is properly set for the proposed MD technique, the correlation output between the MD of m_v and the MD of s_v is found as

$$\begin{aligned} z_v^{(m_v)}[n] = {} & \big[(M_v[n+1] + b_v[n+1]) - (M_v[n] + b_v[n])\big] \\ & \times \big(s_v[n+1] - s_v[n]\big) \\ \simeq {} & \big(M_v[n+1] - M_v[n]\big)\big(s_v[n+1] - s_v[n]\big) \end{aligned} \quad (13)$$

which shows that there is no MO effect.

For the proposed MD technique, the correlation output between the MD of m_h and that of s_h is derived as

$$\begin{aligned} z_h^{(m_v)}[n] = {} & \big[(M_{hx}[n+1] + b_{hx}[n])^2 + (M_{hy}[n+1] + b_{hy}[n])^2 \\ & - (M_{hx}[n] + b_{hx}[n])^2 - (M_{hy}[n] + b_{hy}[n])^2\big] \\ & \times \big(s_{hx}^2[n+1] + s_{hy}^2[n+1] - s_{hx}^2[n] - s_{hy}^2[n]\big) \\ = {} & M_h^{(m_v)}[n] - B_h^{(m_v)}[n] \end{aligned} \quad (14)$$

where

$$\begin{aligned} M_h^{(m_v)}[n] = {} & \big(M_{hx}^2[n+1] + M_{hy}^2[n+1] - M_{hx}^2[n] - M_{hy}^2[n]\big) \\ & \times \big(s_{hx}^2[n+1] + s_{hy}^2[n+1] - s_{hx}^2[n] - s_{hy}^2[n]\big) \end{aligned} \quad (15a)$$

$$\begin{aligned} B_h^{(m_v)}[n] = {} & 2\big(b_{hx}[n](M_{hx}[n+1] - M_{hx}[n]) \\ & + b_{hy}[n](M_{hy}[n+1] - M_{hy}[n])\big) \\ & \times \big(s_{hx}^2[n+1] + s_{hy}^2[n+1] - s_{hx}^2[n] - s_{hy}^2[n]\big). \end{aligned} \quad (15b)$$

From (15b), due to $E[b_{hx}[n]] = 0$ and $E[b_{hy}[n]] = 0$, it is found that $B_h^{(m_v)}$ has a zero mean and variance as

$$E\big[B_h^{(m_v)}[n]\big] = 0 \quad (16a)$$

$$\begin{aligned} \mathrm{Var}\big(B_h^{(m_v)}[n]\big) = {} & E\big[\big(s_{hx}^2[n+1] + s_{hy}^2[n+1] \\ & \quad - s_{hx}^2[n] - s_{hy}^2[n]\big)^2\big] \\ & \times \big(E\big[4b_{hx}^2[n](M_{hx}[n+1] - M_{hx}[n])^2\big] \\ & + E\big[4b_{hy}^2[n](M_{hy}[n+1] - M_{hy}[n])^2\big]\big) \end{aligned} \quad (16b)$$

respectively.

Comparing (9) with (11) and (10b) with (12), it is found that the proposed MD technique has a much larger SOR than the conventional Amp. technique in both the vertical and horizontal measurements. Therefore, it is theoretically found that the proposed MD technique is robust to the time-varying MO and outperforms the conventional Amp. technique. To support this theoretical analysis, we perform simulations to show the SOR with respect to a varying (sinusoidal) MO ranging from 2 to 12 μT at 0.5 Hz. The user velocity and sampling rate are assumed to be 1.5 m/s and 10 Hz, respectively. As shown in Fig. 3, for varying attitude, the proposed MD technique has a much larger SOR than the conventional Amp. technique.

B. Fixed Attitude of Mobile Device

In this section, we analyze the performance of the conventional Amp. technique and that of the proposed MD technique by comparing the SOR for the vertical and horizontal

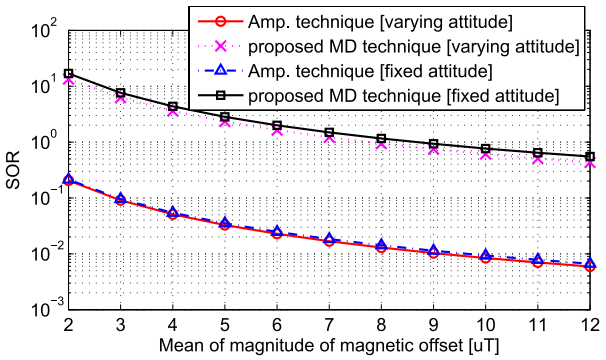

Fig. 3. SOR.

MFI measurements from mobile devices with a fixed attitude and with a fixed vertical axis. The latter may be the case when the mobile device is fixed on a horizontal platform. Therefore, we assume that the vertical MO b_v is time invariant and that the horizontal MO b_h is time invariant or time varying depending on the applications.

For time-invariant vertical MO, $B_v^{(a_f)}$ has a nonzero mean and variance as

$$E\big[B_v^{(a_f)}[n]\big] = b_v E\big[s_v[n]\big] \tag{17a}$$

$$\mathrm{Var}\big(B_v^{(a_f)}[n]\big) = b_v^2\big(E\big[s_v^2[n]\big] - E\big[s_v[n]\big]^2\big) \tag{17b}$$

respectively. For time-invariant horizontal MO, exploiting (6b), $B_h^{(a_f)}$ has a nonzero mean and variance as

$$E\big[B_h^{(a_f)}[n]\big] = \big(b_{hx}^2 + b_{hy}^2\big)E\big[s_{hx}^2[n] + s_{hy}^2[n]\big] \tag{18a}$$

$$\begin{aligned}\mathrm{Var}\big(B_h^{(a_f)}[n]\big) = {} & E\big[(s_{hx}^2[n] + s_{hy}^2[n])^2\big]\big(4b_h^4 + 8b_h^2 E\big[M_h^2[n]\big]\big) \\ & - 2b_h^2 E\big[(s_{hx}^2[n] + s_{hy}^2[n])\big]\end{aligned} \tag{18b}$$

respectively.

As a result, in the presence of a time-invariant MO, the variance of the vertical offset–distortion component (17b) divided by the power of the vertical signal component $M_v^{(a)}[n]$ for the conventional Amp. technique is obtained as

$$P_v^{(a_f)}[n] = b_v^2\big(1 - E\big[s_v[n]\big]^2 / E\big[s_v^2[n]\big]\big). \tag{19}$$

In addition, the variance of the horizontal offset–distortion component (18b) divided by the power of the horizontal signal component $M_h^{(a)}[n]$ for the conventional Amp. technique is derived as

$$\begin{aligned}P_h^{(a_f)}[n] = {} & 4b_h^4 + 8b_h^2 E\big[M_h^2[n]\big] \\ & - \frac{2b_h^2 E\big[(s_{hx}^2[n] + s_{hy}^2[n])\big]}{E\big[(s_{hx}^2[n] + s_{hy}^2[n])^2\big]}.\end{aligned} \tag{20}$$

For the proposed MD technique, $B_v^{(m_f)} = 0$ exploiting the analysis in (13) and from (15b) $B_h^{(m_f)}$ has a mean and a variance as

$$E\big[B_h^{(m_f)}[n]\big] = 0 \tag{21a}$$

$$\begin{aligned}\mathrm{Var}\big(B_h^{(m_f)}[n]\big) = {} & E\big[\big(s_{hx}^2[n+1] + s_{hy}^2[n+1] \\ & - s_{hx}^2[n] - s_{hy}^2[n]\big)^2\big] \\ & \times\big(4b_{hx}^2 E\big[(M_{hx}[n+1] - M_{hx}[n])^2\big] \\ & + 4b_{hy}^2 E\big[(M_{hy}[n+1] - M_{hy}[n])^2\big]\big)\end{aligned} \tag{21b}$$

respectively.

In the presence of a time-invariant MO, the variance of the vertical offset–distortion component is zero, as found in (13)

$$P_v^{(m_f)}[n] = 0 \tag{22}$$

and the variance of the horizontal offset–distortion component (21b) divided by the horizontal signal component (15a) is obtained as

$$\begin{aligned}P_h^{(m_f)}[n] = {} & 4b_{hx}^2 E\big[(M_{hx}[n+1] - M_{hx}[n])^2\big] \\ & + 4b_{hy}^2 E\big[(M_{hy}[n+1] - M_{hy}[n])^2\big].\end{aligned} \tag{23}$$

Comparing (19) with (22) and (20) with (23), it is found that the proposed MD technique theoretically has much larger SOR than the conventional Amp. technique for the vertical and horizontal measurements, in the presence of time-invariant MO, and that the proposed MD technique is robust to time-invariant MO and outperforms the conventional Amp. technique. To support this theoretical analysis, we perform simulations to show the SOR with respect to various MO ranging from 2 to 12 μT with fixed attitude, as shown in Fig. 3. In this simulation, the assumed user velocity and sampling rate are 1.5 m/s and 10 Hz, respectively.

III. Fast Pattern Matching Algorithm

When the vertical direction of the smartphones is reliably estimated by the built-in three-axis accelerometer, a pattern matching algorithm can exploit the Mahalanobis distance [26] as a normalized cost function for positioning. However, evaluating the Mahalanobis distance involves a matrix inversion, which is computationally expensive when the matrix is large. In addition, the mobile device must evaluate the cost function for all possible location, direction, and velocity hypotheses within a given indoor area, which may require a large computational cost. Since the mobile device has a limited amount of computing capacity and battery, we propose a low computational pattern matching algorithm to evaluate the Mahalanobis distance [26] for a set of vertical and horizontal MFI MDs.

In the following, we assume that a user walks for a distance d ($1\ \mathrm{m} \ll d$) to collect N MFI measurements at N locations along the path, and let $\mathbf{Y} = [\mathbf{m}_v, \mathbf{m}_h]$ be the N by 2 matrix whose first and second columns are N vertical MFI measurements and N horizontal MFI magnitude measurements, respectively, and let $\mathbf{Y}_0$ be the MO-free N by 2 matrix stored in MDB such that

$$\mathbf{Y} = \mathbf{Y}_0 + \mathbf{B} + \mathbf{w} \tag{24}$$

where $\mathbf{B} = [\mathbf{b}_v, \mathbf{b}_h]$ is the N by 2 matrix of vertical and horizontal MOs in the N vertical and horizontal measurements, respectively. The statistical characteristics of $\mathbf{b}_v$ and $\mathbf{b}_h$ are found in Section II for time-varying and time-invariant MOs. The first and second rows of $\mathbf{w}$ are approximated by Additive White Gaussian Noise (AWGN) processes with variance σ_v^2 and $2\sigma_v^2$, respectively [23].

Subtracting the first forward difference of $\mathbf{Y}_0$ from that of $\mathbf{Y}_0$, an error vector is expressed as

$$\begin{aligned}\mathbf{e} &= \mathbf{DY} - \mathbf{DY}_0 \\ &= \mathbf{D}(\mathbf{B} + \mathbf{v})\end{aligned} \tag{25}$$

where

$$\mathbf{D} = \begin{bmatrix} -1 & 1 & 0 & 0 & \dots & 0 & 0 \\ 0 & -1 & 1 & 0 & \dots & 0 & 0 \\ \vdots & \vdots & \vdots & \vdots & \ddots & \vdots & \vdots \\ 0 & 0 & 0 & 0 & \dots & 1 & 0 \\ 0 & 0 & 0 & 0 & \dots & -1 & 1 \end{bmatrix} \tag{26}$$

is the first forward difference operation matrix. Therefore, the variance of the sum of magnetic bias and noise $B[n] + w[n]$ in the nth measurement is found as

$$\sigma_{[n]}^2 = \begin{cases} \sigma_1^2 \big(= \sigma_b^2 + 2\sigma_v^2 \big) & \text{for } 1 \le n \le N \\ \sigma_2^2 \big(= 2\sigma_b^2 + 4\sigma_v^2 \big) & \text{for } N+1 \le n \le 2N. \end{cases} \tag{27}$$

As found, the components of $\mathbf{w}$ in (25) have two different variances depending on n, as in (27).

Therefore, the expression for the normalized cost function (i.e., Mahalanobis distance) for a set of N vertical and horizontal measurements can be derived as

$$\begin{aligned} J(\mathbf{Y}) &= \mathbf{e}^T E[\mathbf{e}\mathbf{e}^T]^{-1}\mathbf{e} \\ &= \mathbf{e}^T \mathbf{P}^{-1}\mathbf{e} \\ &= [\mathbf{B} + \mathbf{v}]^T \mathbf{D}^T \mathbf{P}^{-1} \mathbf{D}[\mathbf{B} + \mathbf{v}] \end{aligned} \tag{28}$$

which requires a matrix inversion, i.e., $\mathbf{P}^{-1}$. Note that since N can be different depending on the required positioning accuracy in practice (for example, larger N for better accuracy), $\mathbf{P}^{-1}$ should be computed whenever N changes, which may be a computationally expensive for a mobile device. To reduce the computational cost in evaluating $J(\mathbf{Y})$, we introduce a low computational and fast algebraic algorithm to compute $\mathbf{D}^T\mathbf{P}^{-1}\mathbf{D}$ in this section.

Let

$$\mathbf{D} = \big[\mathbf{1}_c, \mathbf{D}_2\big] \tag{29}$$

where $\mathbf{1}_c$ and $\mathbf{D}_2$ are a vector representing the first column of $\mathbf{D}$ and a $[(2N-1]) \times (2N-1)]$ rectangular matrix whose nth column is the $(n+1)$th column of $\mathbf{D}$ for $n \in \{1, 2, \dots, 2N-1\}$, respectively, then

$$\begin{aligned} \mathbf{D}^T\mathbf{P}^{-1}\mathbf{D} &= \begin{bmatrix} \mathbf{1}_c^T \\ \mathbf{D}_2^T \end{bmatrix} \mathbf{P}^{-1} [\mathbf{1}_c \quad \mathbf{D}_2] \\ &= \begin{bmatrix} \mathbf{1}_c^T\mathbf{P}^{-1}\mathbf{1}_c & \mathbf{1}_c^T\mathbf{P}^{-1}\mathbf{D}_2 \\ \mathbf{D}_2^T\mathbf{P}^{-1}\mathbf{1}_c & \mathbf{D}_2^T\mathbf{P}^{-1}\mathbf{D}_2 \end{bmatrix}. \end{aligned} \tag{30}$$

In the following, we let Λ represent a diagonal matrix whose element at the nth row and nth column is $\sigma_{[n]}^2$ defined in (27), and let Λ_2 be a $[(2N-1) \times (2N-1)]$ diagonal matrix whose nth diagonal element is the element of Λ at the $(n+1)$th row and the $(n+1)$th column for $n \in \{1, 2, \dots, 2N-1\}$. After some algebraic manipulations, it is derived that

$$\mathbf{1}_c^T\mathbf{P}^{-1}\mathbf{1}_c = \frac{1}{\sigma_{[1]}^2} - \frac{1}{\sigma_{[1]}^4 \big(\sum_{n=1}^{2N} \sigma_{[n]}^{-2} \big)} \tag{31a}$$

$$\mathbf{1}_c^T\mathbf{P}^{-1}\mathbf{D}_2 = -\frac{\Sigma_2}{\sigma_{[1]}^2 \big(\sum_{n=1}^{2N} \sigma_{[n]}^{-2} \big)} \tag{31b}$$

$$\mathbf{D}_2^T\mathbf{P}^{-1}\mathbf{1}_c = -\frac{\Sigma_2^T}{\sigma_{[1]}^2 \big(\sum_{n=1}^{2N} \sigma_{[n]}^{-2} \big)} \tag{31c}$$

$$\mathbf{D}_2^T\mathbf{P}^{-1}\mathbf{D}_2 = \Lambda_2^{-1} - \frac{\Sigma_2^T\Sigma_2}{\Big(\sum_{n=1}^{2N} \sigma_{[n]}^{-2} \Big)} \tag{31d}$$

where

$$\Sigma_2 = \big[\sigma_{[2]}^{-2}, \sigma_{[3]}^{-2}, \dots, \sigma_{[2N]}^{-2}\big]. \tag{32}$$

Using (31a)–(31d) for $\mathbf{D}^T\mathbf{P}^{-1}\mathbf{D}$ (30), a low computational algebraic expression for $J(\mathbf{Y})$ is obtained as

$$\begin{aligned} J(\mathbf{Y}) &= (\mathbf{Y} - \mathbf{Y}_0)^T \left[\Lambda^{-1} - \left(\sum_{n=1}^{2N} \sigma_{[n]}^{-2} \right)^{-1} \Sigma^T\Sigma \right] (\mathbf{Y} - \mathbf{Y}_0) \\ &= \sigma_1^{-2} \sum_{n=1}^{N} (Y[n] - Y_0[n])^2 + \sigma_2^{-2} \sum_{n=N+1}^{2N} (Y[n] - Y_0[n])^2 \\ &\quad - \frac{1}{N(\sigma_1^{-2} + \sigma_2^{-2})} \left[\sum_{n=1}^{N} \frac{Y[n] - Y_0[n]}{\sigma_1^2} \right. \\ &\quad \left. + \sum_{n=N+1}^{2N} \frac{Y[n] - Y_0[n]}{\sigma_2^2} \right]^2 \end{aligned} \tag{33}$$

where

$$\Sigma = \big[\sigma_{[1]}^{-2}, \Sigma_2\big]. \tag{34}$$

Note that the low computational algorithm for $J(\mathbf{Y})$ (33) requires only $\mathcal{O}(N)$ multiplications, whereas the conventional algorithm for $J(\mathbf{Y})$ (28) requires $\mathcal{O}(N^3)$. Note also that for a given measurement rate, N depends on d. The measurement rate should be high enough to see the variation of MFI over a path but should not be too high to have large N in order to reduce the computational cost. On the other hand, d should not be too small so that the measurements contains variations of MFI over a distance. However, since the proposed technique may loose accuracy when there is a significant change in the direction or speed of the user motion, d should not be too large (e.g., $d \gg 10$ m).

IV. Bayesian Filtering for Positioning Process

In this section, we introduce the Bayesian filtering used for mobile device positioning with the proposed technique. The performance results are given in Section V. In the positioning process, the MDB is given and the initial approximate location of the mobile device is assumed to be known within a 5-m radius.

TABLE I
BAYESIAN FILTERING ALGORITHM

Given MDB $\mathbf{Y}_{0,all}$ *and* $k = 1$

Prediction Step

- If $k = 1$, let

$$\overline{bel}(\mathbf{x}_k)\big|_{k=1} = \mathbf{1}_{(\mathbf{x}_1, \mathbf{W})}, \tag{39}$$

where $\mathbf{1}_{(\mathbf{x}_1, \mathbf{W})}$ denotes a uniform distribution over a circular area $\mathbf{W}$ of radius l_w around $\mathbf{x}_1$.

- If $k \neq 1$, compute

$$\overline{bel}(\mathbf{x}_k) = \sum_{\mathbf{x}_{k-1} \subset \mathbf{W}} p(\mathbf{x}_k|\mathbf{x}_{k-1}, \mathbf{u}_k) bel(\mathbf{x}_{k-1}) \tag{40}$$

for all $\mathbf{x}_k$, where $\mathbf{u}_k$ represents user motion, $\mathbf{W}$ is a circular window area of radius l_w around $\mathbf{x}_{k-1}$.

Correction Step

- Obtain measurements $\mathbf{Y}$ and compute

$$bel(\mathbf{x}_k) = \eta p(\mathbf{Y}_k|\mathbf{x}_k) \overline{bel}(\mathbf{x}_k) \tag{41}$$

for all $\mathbf{x}_k$, where η is a normalization factor

- Increase k by 1 and go to the prediction step.

The Bayesian filtering iteratively updates the belief distribution that is posterior probabilities over state variables conditioned on the available data [4]. The positioning procedure with the basic Bayesian filtering consists of two steps: in the prediction step, $\overline{bel}(x_k)$ (i.e., prior distribution) is calculated, and in the correction step, $bel(x_k)$ (i.e., posterior distribution) is calculated from $\overline{bel}(x_k)$ and the likelihood distribution [4]. The pseudoalgorithm of the Bayesian filtering [4] is described in Table I, where the MDB $\mathbf{Y}_{0,all}$ is constructed with measurements at every $l\text{m}^2$ ($l \ll 1$) and the size of the MDB is $[L \times L]$. Initially ($k = 1$), an approximate location of the mobile device is known within a circular region $\mathbf{W}$ of radius l_w centered at $\mathbf{x}_1 (= [x_1, y_1])$. Then initial the belief distribution is a uniform distribution for a certain circular region W centered at $\mathbf{x}_1 (= [x_1, y_1])$ (39). Within a time interval T_0, the kth iteration, starting at $t = t_1 + (k-1)T_0$ (for $k = 1, 2, 3, \ldots$), where t_1 is the time to start the Bayesian filter, the user is moving along a straight path segment, from $\mathbf{x}_{k-1} (= [x_{k-1}, y_{k-1}])$ to $\mathbf{x}_k (= [x_k, y_k])$, that has an unknown direction θ_k, and at the same time, the mobile device collects $N (\ll L)$ samples of vertical and horizontal MFI measurements with a sampling rate $R_M = N/T_0$Hz to build $\mathbf{Y}_k$ (i.e., $\mathbf{Y}$ at $t = t_1 + (k-1)T_0$). We assume that the user is moving with a constant velocity $\mathbf{u}_k$ during a small T_0. The control input $\mathbf{u}_k$ in Table I is the expected velocity and direction $\{\mathbf{u}_k, \theta_k\}$, which are unknown to the algorithm. For the expected velocity and direction, predict the next $k+1$th position based on kth correction results as in (40).

The Bayesian filter tries to find the best match between $\mathbf{Y}_k$ and a subset of $\mathbf{Y}_{0,all}$, $\mathbf{Y}_0|(\mathbf{x}_{k-1}, \theta_k) (= \mathbf{Y}_0|(\overrightarrow{\mathbf{x}_{k-1}\mathbf{x}_k}))$ that is composed of N samples along a possible straight path segment starting from an unknown point in $\mathbf{W}$. Since the user velocity, moving direction, and the exact starting point $\mathbf{x}_{k-1}$ are generally unknown, $\mathbf{Y}_0$ of size N should be collected for various user velocities and moving directions for all possible user locations (i.e., $\mathbf{x}_{k-1} \in \{\mathbf{x}_{k-1}|\overline{bel}(\mathbf{x}_{k-1}) > 0\}$), which increases the computational complexity of the Bayesian filtering.

For the measurement likelihood $p(\mathbf{Y}_t|\mathbf{x}_t)$ in (41), we employ the inverse of the proposed MD-based cost function, i.e., $J(\mathbf{Y})^{-1}$ (33), so that the maximum of the measurement likelihood indicates the most probable location of the mobile device $\mathbf{x}_t$ as

$$F_{\text{MD}}(\mathbf{Y}_k|\mathbf{x}_k) = \frac{1}{J(\mathbf{Y}_k)}. \tag{35}$$

In the following analysis, $F_{\text{MD}}(\mathbf{Y}_k|\mathbf{x}_k)$ denotes the MD-based measurement likelihood function (MD likelihood). In the simulations and tests in Section V, the conventional matching (CM)-based measurement likelihood function (CM likelihood) obtained from the inverse of error-squared

$$F_{\text{CM}}(\mathbf{Y}_k|\mathbf{x}_k) = \frac{1}{(\mathbf{Y}_k - \mathbf{Z}_0)^T (\mathbf{Y}_k - \mathbf{Z}_0)} \tag{36}$$

and a map correlation (MC)-based measurement likelihood function (MC likelihood) introduced in [4]

$$F_{\text{MC}}(\mathbf{Y}_k|\mathbf{x}_k) = \eta_0 \sum_{p=0}^{N-1} (Y(p) - \bar{m})(Z_0(p) - \bar{m}) \tag{37}$$

are used for a comparison, where

$$\begin{aligned} \mathbf{Z}_0 &= \mathbf{Y}_0|(\mathbf{x}_{k-1}, \theta_k) \\ \eta_0 &= \left[\sum_{p=0}^{N-1} (Y(p) - \bar{m})^2 \sum_{p=0}^{N-1} (Z_0(p) - \bar{m})^2 \right]^{\frac{1}{2}} \\ \bar{m} &= \frac{\sum_{p=0}^{N-1} \big(Y(p) + Z_0(p)\big)}{2N}. \end{aligned} \tag{38}$$

After obtaining $p(\mathbf{Y}_t|\mathbf{x}_t)$ in (41), belief distribution in the k-h prediction step is multiplied with $p(\mathbf{Y}_t|\mathbf{x}_t$ for correction as in (41).

V. PERFORMANCE TEST RESULT

In this section, we show the accuracy and reliability of the proposed three-axis accelerometer-based roll and pitch angle estimation with the experimental results, in comparison with those of the three-axis gyroscope based estimation. In addition, we test the three measurement likelihood functions, $F_{\text{MD}}(\mathbf{Y}_k|\mathbf{x}_k)$ (35), $F_{\text{CM}}(\mathbf{Y}_k|\mathbf{x}_k)$ (36), and $F_{\text{MC}}(\mathbf{Y}_k|\mathbf{x}_k)$ (37), for positioning with the Bayesian filter in Table I.

In the field tests, a calibrated three-axis magnetometer, Honeywell HMR2300 [27], is used to build the MDB at every 10 cm in the xy horizontal plane, and the total number of samples N used for matching is 60 for all 100 field test runs of about $d = 5.5$ m long. The measurements for the MDB are collected at about 1.5-m height from the floor in two indoor environments within the campus of the Korea Advanced Institute of Science and Technology: a long corridor (about 25 m long) in a concrete building and a wide indoor floor (about $[25 \times 20]$ m^2) in a glass–wall building. Note that the MDB for CM and MC likelihoods contains the MFI magnitude,

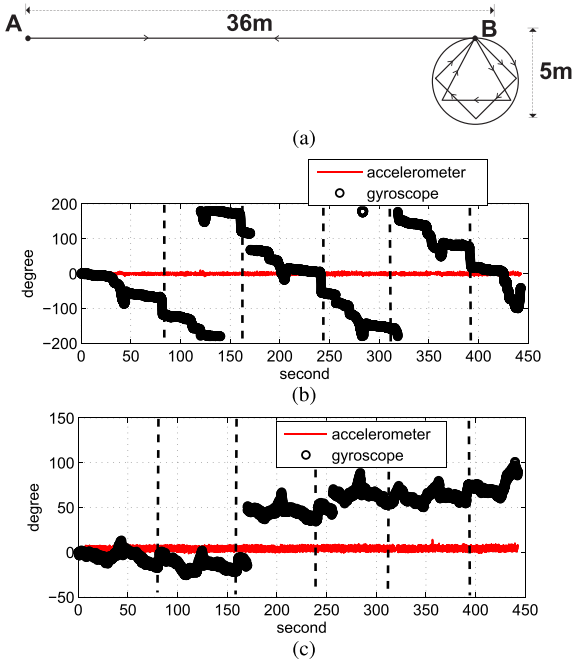

Fig. 4. Performance for estimating the direction of gravity. (a) Moving routes for experiment. (b) Estimated roll angle. (c) Estimated pitch angle.

since the CM and MC likelihoods use the magnitudes of MFI for pattern matching, while for the proposed MD likelihood, we build an MDB using the horizontal MFI magnitude and vertical MFI amplitude.

To test the robustness of the proposed technique to unknown MO, we use distorted MFI measurements for the measurements from the three-axis magnetometer in a smartphone corrupted by MO, where the distorted measurements are the true MFI measurements, obtained with the Honeywell HMR2300, added with an unknown time-varying offset. Since the user velocity is unknown and the locations where the three-axis magnetometer in the user's smartphone collects MFI measurements are unknown, we apply a linear interpolation to the MDB to generate samples for the smartphone and the MDB values actually used for the pattern matching. In addition, to exaggerate the imperfect estimation of the vertical direction with a three-axis accelerometer, we assume that the accelerometer has Gaussian distributed random bias with a mean of 0.01 g and a standard deviation of 0.1 g, which is about ten times larger than that of accelerometers used in commercial smartphones [28], where $g = 9.8$ m/s^2.

To verify the idea of using an accelerometer to estimate the direction of gravity instead of using a power consuming gyroscope to estimate the attitude of the smartphone, we perform real field tests and show the roll and pitch angles estimated by the accelerometer and gyroscope for the comparison in Fig. 4. In the field tests, we walk from point A to point B along a straight path of about 36 m, follow a closed path to turn back to point B, walk from point B to point A, and turn around to complete a collection of magnetometer measurements with a smartphone held in one hand stably, as shown in Fig. 4(a). Six sets of measurements are collected consecutively using a Samsung Galaxy S5 [29] and the types of closed paths are circular, triangular, and diamond shaped in an order that is repeated two

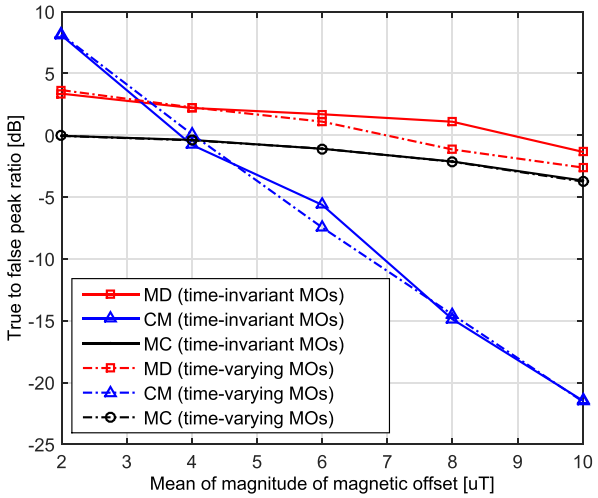

Fig. 5. Performance of robustness for MOs.

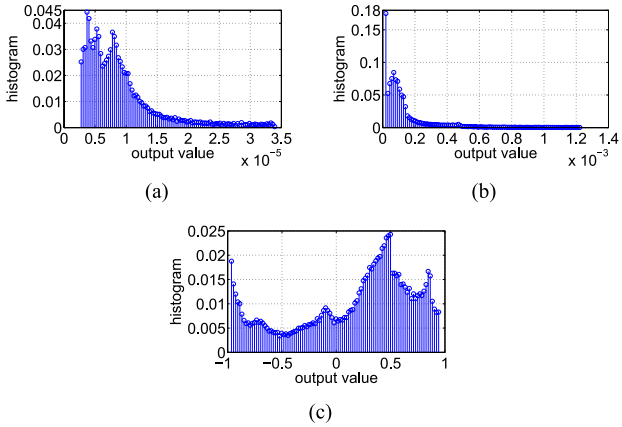

Fig. 6. Histogram of the cost functions, i.e., the inverse of the likelihood functions. (a) MD. (b) CM. (c) MC.

times. As shown in Fig. 4(b) and (c), the estimated roll and pitch angles with the three-axis accelerometer do not drift, while those with the three-axis gyroscopes drift significantly.

To demonstrate the robustness of the proposed technique to time-varying and time-invariant MOs of various amplitudes, we run the Bayesian filter employing the MD likelihood with field measurements. In Fig. 5, the performance of robustness to unknown MOs is measured in terms of the true-to-false peak ratio with respect to the mean magnitude of MOs. The CM likelihood $F_{\mathrm{CM}}(\mathbf{Y}_k|\mathbf{x}_k)$ shows the poorest performance as the magnitude of the MO increases. The performance of the MC likelihood $F_{\mathrm{MC}}(\mathbf{Y}_k|\mathbf{x}_k)$ is also not reliable, as there are often false peaks higher than the true peak in the pattern matching result. As expected, the proposed MD likelihood $F_{\mathrm{MD}}(\mathbf{Y}_k|\mathbf{x}_k)$ shows a superior performance to the others in all the six tests.

The performance of the three likelihood functions can be compared with their histograms obtained for a time-varying MO with a mean magnitude of 4 μT, as shown in Fig. 6. Comparing the histogram for the proposed MD likelihood shown in Fig. 6(a) and that for the CM likelihood shown in Fig. 6(b), we find that the CM likelihood has most of likelihood very small. However, from the results shown in Fig. 5, it can be found that the CM likelihood generates false peaks that are stronger than the true peaks. In contrast, the histogram of the

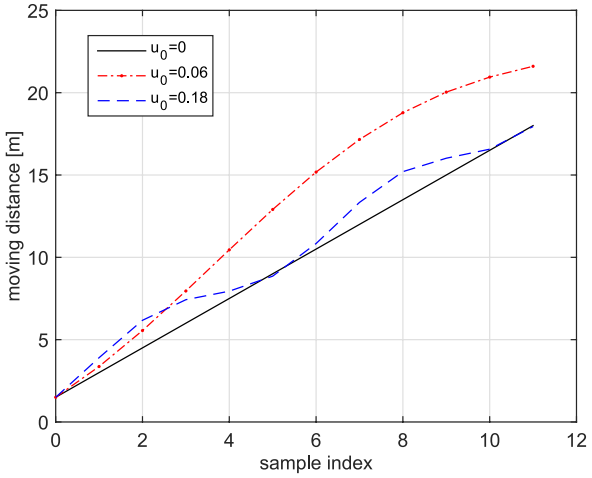

Fig. 7. Moving distance for various u_0.

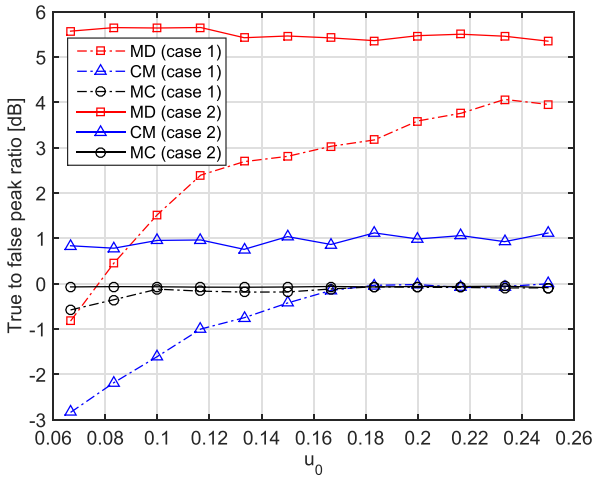

Fig. 8. Performance of robustness for varying velocity.

MC likelihood is relatively flat, and consequently, the true peak to false peak ratio is about 1 very often, which explains that the true-to-false-peak-ratio is equal or less than 0 dB, as shown in Fig. 5.

Since the user velocity is unknown and time varying but can be assumed to be constant during a small time interval T_0 in practice, we test the robustness of the three likelihood functions to the unknown slowly varying user velocity. In the pattern matching for the unknown user velocity at each time interval, multiple user velocity hypotheses are considered in computing the likelihood functions. In Figs. 8 and 9, we show the robustness of the three likelihood functions to the time-varying user velocity u for two cases: case 1: $u = \sin(2\pi u_0 n) + 1$ m/s and case 2: $u = 0.5\sin(2\pi u_0 n) + 1$ m/s, where u_0 varies from 0.06 to 0.24 and n represents the sampling index ($n = 1, 2, \ldots, 11$) [22]. For a good match between the measurement and the map data, the assumed user velocity should be the same as the true user velocity. Fig. 7 shows the moving distance for various u_0. As shown, the difference between the assumed moving distance (i.e., for $u_0 = 0$) and the actual moving distance (i.e., for $u_0 \neq 0$) increases as u_0 decrease, based on which the results in Figs. 8 and 9 can be analyzed.

Fig. 8 shows the average true-to-false peak ratio (dB) of the three likelihood functions; the three likelihood functions show robustness to small velocity variations (case 2), but the average true-to-false peak ratios of the three likelihood functions are worse for case 1 than case 2. Similar to the results in Fig. 5, the MC likelihood function is almost unaffected by MO variation; however, the CM likelihood and the proposed MD likelihood functions have large degradation for small u_0. The CM and the proposed MD likelihood functions are unaffected for $u_0 \geq 0.16$ and $u_0 \geq 0.22$, respectively. In general, all three likelihood functions suffer from the time-varying velocity for smaller u_0, while the proposed MD likelihood function shows the best performance in all simulation results; the performance degradation of the proposed MD likelihood function is the largest among the three.

Fig. 9 shows the instantaneous positioning accuracy estimated from the three likelihood functions for two varying user velocities (i.e., cases 1 and 2) in terms of root-mean-square

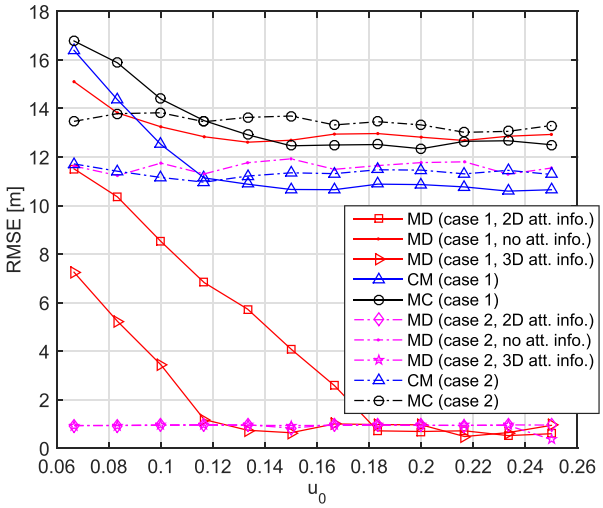

Fig. 9. RMSE of position estimation error.

error (RMSE). For the proposed MD likelihood function, the performances according to the amount of attitude information (i.e., no attitude information: no att. info. in the legend, 2-D attitude information: 2-D att. info. in the legend, and 3-D attitude information: 3-D att. info. in the legend) are compared. The case of 2-D attitude information is when the direction of gravity is estimated with the three-axis accelerometer, as proposed in this paper, and the case of 3-D attitude information is when both a three-axis gyroscope and a three-axis accelerometer are used. The results show a pattern somewhat similar to the results in Fig. 8; the three likelihood functions are robust to small velocity variations (case 2) but show performance degradation for large velocity variation (case 1). The performance of the proposed technique is much better than those of the others except for case 1 and when no attitude information is available. It is interesting that in case 2, the proposed MD likelihood with only vertical directional information and that with 3-D attitude information have almost the same performance and that in case 1, there is a larger difference for smaller u_0. Overall, we find that the proposed MD likelihood function with the three-axis accelerometer shows much better performance than that with no attitude information and shows a slightly worse performance than

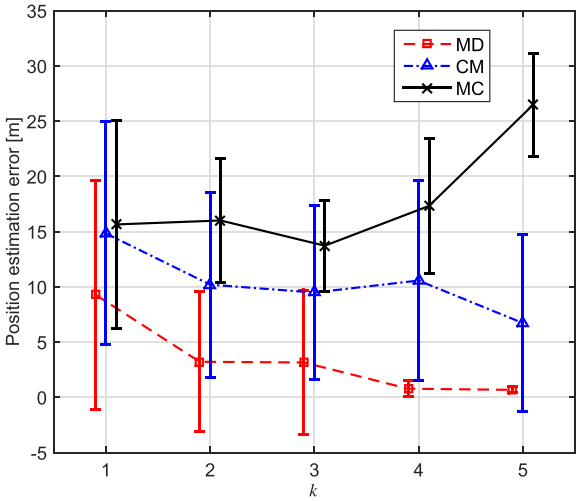

Fig. 10. Verification of the matching functions using the Bayesian filter.

that with 3-D attitude information. However, the gyroscope consumes in excess of ten times more [13] power than the accelerometer, and the estimation uncertainty of the gyroscope grows quickly.

Fig. 10 shows the positioning performance of the Bayesian filter shown in Table I for the three likelihood functions tested with field measurement data. The statistics shown in Fig. 10 are the mean and the standard deviation of positioning errors after a user walks about 5.5 m during T_0. The Bayesian filter with the MC likelihood function shows that the position estimation error is increasing, possibly due to the false peaks, and the Bayesian filter with the CM likelihood function shows that the position estimation becomes slightly better during $K = 5$. In both cases, the position uncertainty is not decreasing. In contrast, the Bayesian filter with the proposed MD likelihood function achieves the highest performance; both the mean positioning error and the uncertainty (the standard deviation) decrease as k increases. Note that for $k > 3$, the mean and the uncertainty of the positioning error with the proposed technique become very small.

VI. Conclusion

A vertical and horizontal magnetic fingerprint MD based pattern matching technique for indoor positioning has been proposed in this paper. It has been shown that the MD enhances the robustness of the pattern matching algorithm to the unknown MO. Furthermore, utilizing the vertical and horizontal magnetic fingerprints obtained with accelerometers and magnetometers for positioning is power efficient and achieves a similar performance to that realized when gyroscopes, accelerometers, and magnetometers are all used. In addition, it has been found that the proposed low computational pattern matching algorithm provides superior computational savings to other conventional pattern matching algorithms. The proposed technique consumes low power and is computationally efficient, and robust to unknown MO and provides strong positioning performance with magnetic fingerprint measurements.

References

[1] H. Liu, H. Darabi, P. Banerjee, and J. Liu, "Survey of wireless indoor positioning techniques and systems," *IEEE Trans. Syst., Man, Cybern. C, Appl. Rev.*, vol. 37, no. 6, pp. 1067–1080, Nov. 2007.

[2] M. Kok, J. D. Hol, and T. B. Schön, "Indoor positioning using ultrawideband and inertial measurements," *IEEE Trans. Veh. Technol.*, vol. 64, no. 4, pp. 1293–1303, Apr. 2015.

[3] S. Tomic, M. Beko, and R. Dinis, "RSS-based localization in wireless sensor networks using convex relaxation: Noncooperative and cooperative schemes," *IEEE Trans. Veh. Technol.*, vol. 64, no. 5, pp. 2037–2050, May 2015.

[4] S. Thrun, W. Burgard, and D. Fox, *Probabilistic Robotics*. London, U.K.: MIT Press, 2006.

[5] J. Haverinen and A. Kemppainen, "A global self-localization technique utilizing local anomalies of the ambient magnetic field," in *Proc. IEEE Int. Conf. Robot. Autom.*, May 2009, pp. 3142–3147.

[6] J. Bird and D. Arden, "Indoor navigation with foot-mounted strapdown inertial navigation and magnetic sensors [emerging opportunities for localization and tracking]," *IEEE Wireless Commun.*, vol. 18, no. 2, pp. 28–35, Apr. 2011.

[7] C.-W. Tan and S. Park, "Design of accelerometer-based inertial navigation systems," *IEEE Trans. Instrum. Meas.*, vol. 54, no. 6, pp. 2520–2530, Dec. 2005.

[8] S. Suksakulchai, S. Thongchai, D. M. Wilkes, and K. Kawamura, "Mobile robot localization using an electronic compass for corridor environment," in *Proc. IEEE Int. Conf. Syst., Man, Cybern.*, vol. 5. Oct. 2000, pp. 3354–3359.

[9] B. Li, T. Gallagher, A. G. Dempster, and C. Rizos, "How feasible is the use of magnetic field alone for indoor positioning?" in *Proc. Int. Conf. Indoor Positioning Indoor Navigat. (IPIN)*, Nov. 2012, pp. 1–9.

[10] S.-E. Kim, Y. Kim, J. Yoon, and E. S. Kim, "Indoor positioning system using geomagnetic anomalies for smartphones," in *Proc. Int. Conf. Indoor Positioning Indoor Navigat.*, Nov. 2012, pp. 1–5.

[11] A. Saxena and M. Zawodniok, "Indoor positioning system using geomagnetic field," in *Proc. IEEE Instrum. Meas. Technol. Conf. (I2MTC)*, May 2014, pp. 572–577.

[12] B. Gozick, K. P. Subbu, R. Dantu, and T. Maeshiro, "Magnetic maps for indoor navigation," *IEEE Trans. Instrum. Meas.*, vol. 60, no. 12, pp. 3883–3891, Dec. 2011.

[13] T. Park, J. Lee, I. Hwang, C. Yoo, L. Nachman, and J. Song, "E-Gesture: A collaborative architecture for energy-efficient gesture recognition with hand-worn sensor and mobile devices," in *Proc. 9th ACM Conf. Embedded Netw. Sensor Syst.*, Seattle, WA, USA, Nov. 2011, pp. 260–273.

[14] A. Thiagarajan, L. Ravindranath, H. Balakrishnan, S. Madden, and L. Girod, "Accurate, low-energy trajectory mapping for mobile devices," in *Proc. NSDI*, Boston, MA, USA, Mar. 2011, pp. 267–280.

[15] E. Dorveaux, D. Vissière, A.-P. Martin, and N. Petit, "Iterative calibration method for inertial and magnetic sensors," in *Proc. 48th IEEE Conf. Decision Control*, Dec. 2009, pp. 8296–8303.

[16] D. Gebre-Egziabher, G. H. Elkaim, J. D. Powell, and B. W. Parkinson, "Calibration of strapdown magnetometers in magnetic field domain," *J. Aerosp. Eng.*, vol. 19, no. 2, pp. 87–102, Apr. 2006.

[17] C. Konvalin, "Compensating for tilt, hard-iron, and soft-iron effects," *Sens. Mag. Online*, pp. 1–11, Dec. 2009. [Online]. Available: http://www.sensorsmag.com/sensors/motion-velocity-displacement/compensating-tilt-hard-iron-and-soft-iron-effects-6475

[18] V. Renaudin, H. Afzal, and G. Lachapelle, "Complete triaxis magnetometer calibration in the magnetic field domain," *J. Sensors*, vol. 2010, pp. 967245-1–967245-10, Dec. 2010.

[19] R. Berkvens, "Feasibility of geomagnetic localization and geomagnetic RatSLAM," *Int. J. Adv. Syst. Meas.*, vol. 7, nos. 1–2, pp. 44–56, 2014.

[20] T. Ozyagcilar. (2013). *Calibrating an eCompass in the Presence of Hard- and Soft-Iron Interference*. [Online]. Available: http://www.freescale.com/files/sensors/doc/app_note/AN4246.pdf

[21] T. Ozyagcilar, "Layout recommendations for PCBs using a magnetometer sensor," Freescale Semicond., Austin, TX, USA, Appl. Note AN4247, May 2011.

[22] J. Liu, R. Chen, L. Pei, R. Guinness, and H. Kuusniemi, "A hybrid smartphone indoor positioning solution for mobile LBS," *Sensors*, vol. 12, no. 12, pp. 17208–17233, 2012.

[23] S. A. H. Tabatabaei, A. Gluhak, and R. Tafazolli, "A fast calibration method for triaxial magnetometers," *IEEE Trans. Instrum. Meas.*, vol. 62, no. 11, pp. 2929–2937, Nov. 2013.

[24] J. Chung, M. Donahoe, C. Schmandt, I.-J. Kim, P. Razavai, and M. Wiseman, "Indoor location sensing using geo-magnetism," in *Proc. 9th Int. Conf. Mobile Syst., Appl., Services*, 2011, pp. 141–154.

[25] X. Yun, E. R. Bachmann, and R. B. McGhee, "A simplified quaternion-based algorithm for orientation estimation from earth gravity and magnetic field measurements," *IEEE Trans. Instrum. Meas.*, vol. 57, no. 3, pp. 638–650, Mar. 2008.

[26] P. C. Mahalanobis, "On the generalized distance in statistics," *Proc. Nat. Inst. Sci. India*, vol. 2, no. 1, pp. 49–55, 1936.
[27] *Smart Digital Magnetometer, HMR2300*. [Online]. Available: https://aerospace.honeywell.com/products/navigation-and-sensors/3-axis-magnetometer
[28] R. Z. Amick, J. A. Patterson, and M. J. Jorgensen, "Sensitivity of tri-axial accelerometers within mobile consumer electronic devices: A pilot study," *Int. J. Appl. Sci. Technol.*, vol. 3, no. 2, pp. 97–100, Feb. 2013.
[29] *Samsung Galaxy S5*. [Online]. Available: https://en.wikipedia.org/wiki/Samsung_Galaxy_S5

Binhee Kim (M'15) received the B.S. and M.S. degrees in electrical engineering and the Ph.D. degree from the Korea Advanced Institute of Science and Technology (KAIST), Daejeon, South Korea, in 2008, 2010, and 2015, respectively.

She is currently a Researcher with the CCS Graduate School for Green Transportation, KAIST. Her current research interests include radar signal processing, global navigation satellite system (GNSS) signal processing, and detection and estimation for navigation systems.

Seung-Hyun Kong (M'06–SM'16) received the B.S. degree in electronics engineering from Sogang University, Seoul, South Korea, in 1992, the M.S. degree in electrical engineering from Polytechnic University, New York, NY, USA, in 1994, and the Ph.D. degree in aeronautics and astronautics from Stanford University, Stanford, CA, USA, in 2006.

He was with Samsung Electronics Inc., Suwon, South Korea, and Nexpilot Inc., Seoul, from 1997 to 2004, where his research interests included wireless communication systems and universal mobile telecommunication system mobile positioning technologies. In 2006 and from 2007 to 2009, he was a Staff Engineer with Polaris Wireless Inc., Santa Clara, CA, USA, and Corporate Research and Development, Qualcomm Inc., San Diego, CA, USA, respectively, where his research interests included assisted-GNSS and wireless positioning technologies, such as wireless location signature and mobile-to-mobile positioning technologies. Since 2010, he has been with the Korea Advanced Institute of Science and Technology, Daejeon, South Korea, where he is currently an Associate Professor with the CCS Graduate School for Green Transportation. His current research interests include next generation GNSS, advanced signal processing for navigation systems, and vehicular communication systems.